RSC Advances

PAPER

View Article Online
View Journal | View Issue

Cite this: *RSC Adv.*, 2014, **4**, 3974

Size-controlled silver nanoparticles synthesized over the range 5–100 nm using the same protocol and their antibacterial efficacy†

Shekhar Agnihotri,[a] Soumyo Mukherji[abc] and Suparna Mukherji*[ad]

Received 20th August 2013
Accepted 22nd October 2013

DOI: 10.1039/c3ra44507k

www.rsc.org/advances

A systematic and detailed study for size-specific antibacterial efficacy of silver nanoparticles (AgNPs) synthesized using a co-reduction approach is presented here. Nucleation and growth kinetics during the synthesis process was precisely controlled and AgNPs of average size 5, 7, 10, 15, 20, 30, 50, 63, 85, and 100 nm were synthesized with good yield and monodispersity. We found the bacteriostatic/bactericidal effect of AgNPs to be size and dose-dependent as determined by the minimum inhibitory concentration (MIC) and minimum bactericidal concentration (MBC) of silver nanoparticles against four bacterial strains. Out of the tested strains, *Escherichia coli* MTCC 443 and *Staphylococcus* aureus NCIM 5201 were found to be the most and least sensitive strains regardless of AgNP size. For AgNPs with less than 10 nm size, the antibacterial efficacy was significantly enhanced as revealed through delayed bacterial growth kinetics, corresponding MIC/MBC values and disk diffusion tests. AgNPs of the smallest size, *i.e.*, 5 nm demonstrated the best results and mediated the fastest bactericidal activity against all the tested strains compared to AgNPs having 7 nm and 10 nm sizes at similar bacterial concentrations. TEM analysis of AgNP treated bacterial cells showed the presence of AgNPs on the cell membrane, and AgNPs internalized within the cells.

1. Introduction

In recent years, metallic nanoparticles have attracted considerable interest due to their intriguing physicochemical properties, small size and surface plasmon behaviour.[1] Among all, silver nanoparticles (AgNPs) display the highest level of commercialization[2] and account for 55.4% of the total nanomaterial-based consumer products available in the market (313, out of 565 products).[3,4] Silver nanoparticles have been utilized in diverse domains including optoelectronics, biosensors, catalysis, surface enhanced Raman scattering (SERS) and, as antimicrobials.[5–7] Most importantly, silver's antimicrobial nature has been extensively exploited owing to its oligodynamic action,[8] broad spectrum killing,[9] and lower possibility for development of microbial resistance against it.[10] As a result, silver in the nano size range has emerged as the most exploited nano-antimicrobial in consumer products such as cosmetics, textiles, dietary supplements, food packaging, surgical coatings, medical implants, and water disinfection applications.[8–16] Previous studies have demonstrated their antimicrobial nature to be size[13] and shape dependent,[14] where smaller nanoparticles displayed better antimicrobial activity. As far as shape is concerned, truncated-triangular nanoparticles appeared to be more effective for microbial killing. However, spherical nanoparticles are still considered to be the best-suited for practical applications in either colloidal form, or immobilized state.[12,15,16]

Despite considerable success in synthesizing AgNPs with different dimensions and size ranges, many of the reported methods have certain limitations in terms of their control over shape, size and stability in the dispersion system.[17] With few exceptions, borohydride-mediated reduction has been employed for the synthesis of dispersible silver nanoparticles.[18] It is worth mentioning that earlier researchers have found it difficult to achieve nanoparticles below 10 nm with high monodispersity and stability.[19–22] For small sized nanoparticles, an excess of strong reducing agent for example, sodium borohydride ($NaBH_4$) is desired, which facilitates instant nuclei generation, resulting in the formation of monodispersed and uniform sized silver colloids. However, it is not easy to obtain larger-sized nanoparticles employing borohydride reduction.[23,24]

[a]*Centre for Research in Nanotechnology and Science, Indian Institute of Technology-Bombay, Powai, Mumbai 400076, India. E-mail: mitras@iitb.ac.in; Fax: +91-22-2576-4650; Tel: +91-22-2576-7854*

[b]*WRCBB, Department of Biosciences and Bioengineering, Indian Institute of Technology-Bombay, Powai, Mumbai 400076, India*

[c]*Centre of Excellence in Nanoelectronics, Indian Institute of Technology-Bombay, Powai, Mumbai 400076, India*

[d]*Centre for Environmental Science and Engineering, Indian Institute of Technology-Bombay, Powai, Mumbai 400076, India*

† Electronic supplementary information (ESI) available: MIC/MBC details, effect of temperature and pH on AgNP synthesis, XRD analysis, TEM images of bacterial cells and table showing various characterization results. See DOI: 10.1039/c3ra44507k

On the other hand, the weaker reducing agent trisodium citrate (TSC) contributes to the formation of relatively large silver nanoparticles, having a wider size distribution. It can also result in a variation in the shape of the nanoparticles *i.e.* spherical nanoparticles are accompanied with undesired generation of rods, cubes, and triangles.[7,25] Thus, using either of the reducing agents, it may be difficult to synthesize silver nanoparticles both, above 50 nm and below 10 nm having a well-defined shape with desired monodispersity. The co-reduction method employing two different reductants (*i.e.*, $NaBH_4$ and TSC) may offer better control on nucleation and growth of nanoparticles.[7,26] This may aid in the synthesis of different sizes of AgNPs using slight variations in the same protocol.

The preparation, characterization and size-specific antibacterial efficacy of silver nanoparticles over a wide size range is described in this article. We refer to a facile, one pot synthesis for the generation of stabilized AgNPs over a wide size range (5–100 nm) achieved by varying the reaction conditions. The proposed dual thermal treatment encourages fast nucleation followed by growth of silver nanoparticles at approximately the same rate, resulting in relatively monodispersed nanoparticles. Also, a variation in pH of the reaction medium facilitated fine tuning of particle morphology from quasi-spherical to nearly spherical shape.[27] Though in recent times few studies have evaluated the size-dependent antimicrobial activity of silver nanoparticles,[28–31] a detailed and substantial study to explore the entire size range from 5–100 nm, is lacking. The current study also investigates a size-selective comparison of their antimicrobial activity against various Gram-positive and Gram-negative bacterial strains. A comprehensive study of antimicrobial activity was made on the basis of bacterial growth kinetics using different amounts of silver nanoparticles, along with MIC/MBC values determined based on liquid cultures using different sizes of silver nanoparticles. While we limit our study to the antibacterial application, relatively larger nanoparticles synthesized using our method can potentially be exploited for other interesting purposes, such as, SERS based diagnostics, bio-sensing, and bio-imaging.

2. Experimental

2.1 Materials

Silver nitrate (>99.9% pure), sodium borohydride ($NaBH_4$, >99% pure), trisodium citrate (TSC, ≥99% pure), and sodium hydroxide were purchased from Merck (India). Ethyl alcohol and acetone were obtained from Merck (Germany) and were used at the desired dilutions. All reagents supplied were of analytical grade and were used without further purification. Throughout the procedures, double deionized (DI) water (with a measured resistivity of 18.2 MΩ cm^{-1}) was used. The antibacterial experiments were carried out using various bacterial strains. *Escherichia coli* MTCC 443 (ATCC 25922), *Escherichia coli* MTCC 739 (ATCC 10536) and *Bacillus subtilis* MTCC 441 (ATCC 6633) were originally procured from the Institute of Microbial Technology (Chandigarh, India). The *Staphylococcus aureus* NCIM 5021 (ATCC 25923) strain was obtained from the National Chemical Laboratory (Pune, India). Nutrient media (Himedia Lab. Ltd., Mumbai) was used for evaluating bacterial growth in liquid broth culture, and was supplemented with a 2% bacteriological agar (Himedia Lab. Ltd., Mumbai) to prepare the solid media used in plate culture studies.

2.2 Synthesis of silver nanoparticles

Silver nanoparticles were synthesized employing sodium borohydride ($NaBH_4$) as a primary reductant and, trisodium citrate (TSC), both as secondary reductant as well as stabilizing agent. The reduction processes were carried out at two different temperatures, *i.e.* at 60 °C and 90 °C, mediated predominantly by, sodium borohydride and trisodium citrate, respectively. A typical procedure is as follows: the required volumes of freshly prepared aqueous solutions containing $NaBH_4$ and TSC were mixed and heated to 60 °C for 30 minutes in the dark with vigorous stirring to ensure a homogenous solution. At the end of 30 minutes, the required volume of $AgNO_3$ solution was added drop-wise to the mixture and subsequently, the temperature was further raised to 90 °C. As the temperature reached 90 °C, the pH of the solution was adjusted to 10.5 using 0.1 M NaOH while heating was continued for 20 minutes, until a change of colour was evident. The nanoparticle suspension was allowed to cool at room temperature. In order to remove the unreacted reductants, AgNP suspensions were centrifuged (12 000 rpm, 15 minutes) and washed thrice, followed by redispersion in DI water and were finally stored at 4 °C for future use. For determining the yield of AgNPs, the silver nanoparticles formed (collected by centrifugation at 14 000 rpm, 20 minutes) were dissolved in dilute HNO_3 and the total mass of silver in the form of AgNPs was determined by inductively coupled plasma-atomic emission spectroscopy (ARCOS ICP-AES spectro, Germany). Subsequently, yield was determined as a ratio of mass of silver in the form of nanoparticles to the mass of silver (Ag^+) added to the flask during the synthesis reaction. Table 1 shows the optimized reaction conditions and details pertaining to the synthesis of different sized AgNPs.

2.3 Instrumentation

UV-Vis extinction spectra were recorded using a spectrophotometer (Perkin-Elmer Lambda 35, USA) in absorbance mode (range 200–800 nm) at desired dilutions of silver colloids. The size and morphology of silver nanoparticles were determined by field emission gun-transmission electron microscopy (FEG-TEM, JEOL JEM 2100F, Japan) at an operational voltage of 200 kV. The diffraction ring patterns (SAED), lattice fringes, and *d*-spacing were examined in its high resolution (HRTEM) mode. Particle size distribution was derived from a histogram considering more than 400 particles measured using multiple TEM micrographs. X-Ray diffraction (XRD) analysis was done using a diffractometer (Philips X′pert PRO, The Netherlands) of Cu-K_α wavelength ($\lambda = 1.54$ Å). For XRD analysis, samples were prepared as discussed in our previous study.[12] In brief, colloidal AgNPs were drop cast on an amine functionalized glass surface, followed by drying in vacuum overnight. The samples were scanned over a 2θ range of 20–90° with a step size of 0.017°. Zeta potential of different AgNP colloids was measured using a zeta

Table 1 Designed conditions for the synthesis of different sized silver nanoparticles[a]

Particle size	Silver nitrate (mol dm^{-3})	Sodium borohydride (mol dm^{-3})	Trisodium citrate (mol dm^{-3})	Volume of reactants (ml)	pH	Temp. (T^a–T^b) (°C)	Yield (%)	Particle conc. (particles per ml)
5	1.00×10^{-03}	2.00×10^{-03}	4.28×10^{-03}	*x*48*y*2	10.5	60–90	78.2	1.03×10^{15}
7	1.00×10^{-03}	2.00×10^{-03}	3.55×10^{-03}	*x*48*y*2	10.5	60–90	67.4	3.31×10^{14}
10	1.17×10^{-03}	2.00×10^{-03}	2.00×10^{-03}	*x*48*y*2	10.5	60–90	82.3	1.53×10^{14}
15	1.00×10^{-03}	1.00×10^{-03}	1.06×10^{-03}	*x*48*y*2	10.5	60–90	77.9	3.49×10^{13}
20	1.00×10^{-03}	1.00×10^{-03}	3.55×10^{-03}	*x*48*y*2	10.5	60–90	~84	1.57×10^{13}
30	4.00×10^{-03}	1.00×10^{-03}	3.55×10^{-03}	*x*45*y*5	10.5	60–90	70.5	1.71×10^{13}
50	1.22×10^{-03}	5.00×10^{-04}	2.00×10^{-03}	*x*45*y*5	10.5	60–90	58.4	9.01×10^{11}
63	2.00×10^{-03}	5.00×10^{-04}	3.54×10^{-03}	*x*40*y*10	10.5	60–90	~61	7.25×10^{11}
85	2.00×10^{-03}	5.00×10^{-06}	1.77×10^{-02}	*x*45*y*5	10.5	60–90	68.3	3.43×10^{11}
100	2.00×10^{-03}	5.00×10^{-06}	1.77×10^{-02}	*x*40*y*10	10.5	60–90	64.6	1.99×10^{11}

[a] *x*-total volume of $NaBH_4$ and TSC; *y*-volume of $AgNO_3$ added drop wise to *x*; T^a-first stage temperature, T^b-second stage temperature (°C).

potential analyzer (Zeta pals, Brookhaven, USA). The suspensions were sonicated for 90 s to minimize aggregation of nanoparticles and three zeta potential measurements were performed for two independent samples.

2.4 Antibacterial tests

To examine the minimum inhibitory concentration (MIC), and minimum bactericidal concentration (MBC) of different sized AgNPs, the procedure specified by Ruparelia *et al.*[32] was followed (ESI, S1†). The effect of AgNPs on bacterial growth kinetics was measured at 600 nm, as increase in absorbance using a spectrophotometer. The experiment included a positive control (flask containing AgNPs and nutrient media, without inoculum) and a negative control (flask containing inoculum and nutrient media, without AgNPs). The absorbance values for experimental flasks (containing nutrient media, inoculum and AgNPs) were corrected by deducting the corresponding absorbance values for the positive controls. All the experiments were carried out in triplicate. Disk diffusion tests were done to determine the size-selective bacterial sensitivity towards AgNPs, as marked by their zone of inhibition (ZoI). As discussed by Ruparelia *et al.*,[32] AgNPs impregnated on filter paper disks (~5 mm diameter) were placed on an agar plate having uniform bacterial suspension (*E. coli.* MTCC 443, 10^4 to 10^5 CFU ml^{-1}). The culture plates were then incubated at 35 °C for 24 hours and the ZoI was measured using photographic images of the agar plates having a clear zone.

The interaction between AgNPs and bacteria and thereby, the mechanism of their bactericidal action was illustrated by treating *E. coli* (MTCC 443, ~10^8 CFU ml^{-1}) with 10 nm AgNPs for 6 hours. The treated cells were centrifuged (10 000 rpm, 10 min.), and washed with DI water to ensure complete removal of colloidal AgNPs from the surface of bacteria. This was followed by a series of pre-treatment procedures required for the microscopic analysis following Morones *et al.*[13] with a few modifications and analysis under FEG-TEM. For FEG-SEM analysis (JEOL JSM-7600F, Japan) samples were drop casted on the carbon coated copper grids, dried at room temperature and were examined without any conductive coating (gold/platinum sputtering).

3. Results and discussion

Silver nanoparticles of different size ranges were synthesized using sodium borohydride and trisodium citrate as reducing agents. The optimized conditions for synthesis of various sizes of AgNP are listed in Table 1. Controlled synthesis of nanoparticles was based on the co-reduction approach using a two stage thermal treatment (Fig. 1). The initial reduction was performed using $NaBH_4$ at 60 °C (stage I) which induced generation of a large number of silver nanoparticles. At this stage, the reduction of silver cations caused the formation of new silver nuclei. This is the dominant process while Ostwald ripening of the formed silver nuclei is only a subsidiary process. Silver nanoparticles formed at the initial stage subsequently participated in the growth process, where TSC-mediated reduction of unspent Ag ions was favoured at the higher temperature, *i.e.*, 90 °C, prevailing in stage II. TSC was, however introduced with $NaBH_4$ during the initial stage. At the lower temperature prevailing in stage I, TCS primarily passivates the nanoparticles and prevents their agglomeration. An adequate $NaBH_4$ to TSC ratio was critical to control the nucleation and growth processes in the two stage co-reduction approach.

Analyzing the reaction conditions for the different sized silver nanoparticles, $NaBH_4$ demonstrated its predominant role for the synthesis of AgNPs having the size range 5–20 nm (ESI, Fig. S2†). On the other hand, TSC was the predominant reducing agent for synthesis of AgNPs of range 60–100 nm. For nanoparticles in the size range 25–60 nm, both $NaBH_4$ and TSC may work concurrently to reduce Ag^+ and form nanoparticles. By varying the temperature, we controlled the reducing ability of sodium borohydride and TSC and produced the most stable "initial" and "final" sols at 60 °C and 90 °C, respectively (ESI, Fig. S3†). The co-reduction approach gave a better balance between nucleation and growth of AgNPs and therefore, synthesis of size controlled silver nanoparticles could be achieved.[7] Moreover, the size and morphology could be precisely tuned by controlling the reduction rate during the second stage with an optimal pH of 10.5 (ESI, Fig. S4†). Thus, this pH was maintained throughout for synthesis of silver nanoparticles of various sizes.

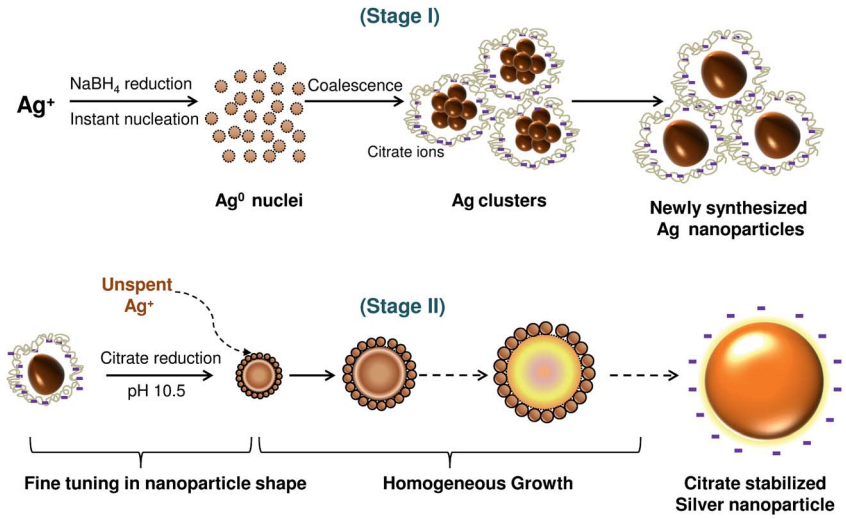

Fig. 1 Schematic representation of size-controlled silver nanoparticles synthesized employing the co-reduction approach.

3.1 Characterization of silver nanoparticles

As shown in Fig. 2a, silver nanoparticles exhibit a sharp extinction peak at 393, 394, 398, 401, 406, 411, 420, 429, 449, and 462 nm wavelength for silver nanoparticles with the average sizes 5, 7, 10, 15, 20, 30, 50, 63, 85, and 100 nm, respectively. As predicted, the absorption maxima of AgNPs shifted to longer wavelength with increase in AgNP size. The full width at half maximum (FWHM) of the corresponding peaks determines dispersity of the nanoparticles, where a large FWHM is attributed to peak broadening and hence, polydispersity. As the size of AgNPs increased from 5 to 30 nm, FWHM values increased from 55 to 85 nm. Further increase in nanoparticle size from 50 to 100 nm yielded significant peak broadening with an increase in FWHM from 138 to 162 nm, respectively. The peak broadening was however unavoidable since a higher concentration of reactants was required for synthesizing larger silver nanoparticles (≥50 nm). The distinctive colour of various silver colloids is also shown in Fig. 2b.

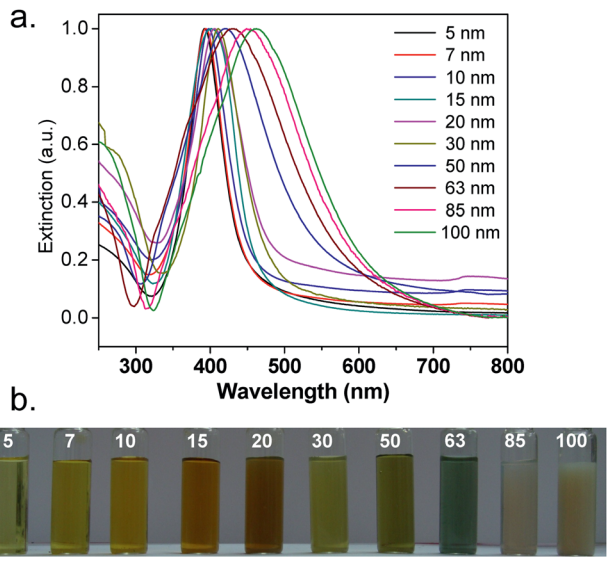

Fig. 2 (a) UV-Vis extinction spectra and (b) the distinctive colour of different sized silver nanoparticles.

The size and morphology of various AgNPs observed using FEG-TEM is shown in Fig. 3. For AgNPs of varying size, most of the nanoparticles were found to be spherical and monodispersed. Table S5† provides details on particle size range determined using TEM analysis. The selected-area electron diffraction (SAED) patterns demonstrated the concentric diffraction rings as bright spots corresponding to the presence of (111), (200), (220), (311), and (222) planes of the face-centered cubic (fcc) silver nanoparticles. The crystalline nature of a single particle was further investigated by means of high resolution (HRTEM) micrographs which showed the presence of lattice fringes with the *d*-spacing value. For silver nanoparticles with the average size 5 and 7 nm, most of the population consisted of single crystalline AgNPs with a *d*-spacing of 2.02 Å, which corresponds to the (200) plane of silver. In contrast, the corresponding diffraction pattern (SAED) indicates that Ag(5) and Ag(7) did not exist as single crystal. Due to instrument limitations, it was not possible to assign the diffraction spots to a particular pattern associated with the face centered cubic (fcc) crystalline silver.[33] In addition to this, the coexistence of a few larger nanoparticles may contribute to the secondary diffraction spots, owing to the presence of twinned crystals (ESI, Fig. S6†). The transformation of single crystalline AgNPs to multiple twinned particles indicates that silver nuclei/particles formed at the first stage undergo Ostwald ripening in the second stage and are transformed into larger silver nanoparticles, thus completing the growth process.[34] For silver nanoparticles with higher average particle size (≥10 nm), HRTEM images showed the presence of multiple-twinned crystalline planes. In Fig. 3c, Ag(10) showed a five-fold multiple twinned decahedron crystal, which is favored for fcc growth of silver.[34]

The crystallite size of different sized silver nanoparticles was also calculated by XRD analysis (using Scherrer's equation, with (111) as the most intense plane), as shown in Fig. S7† of ESI

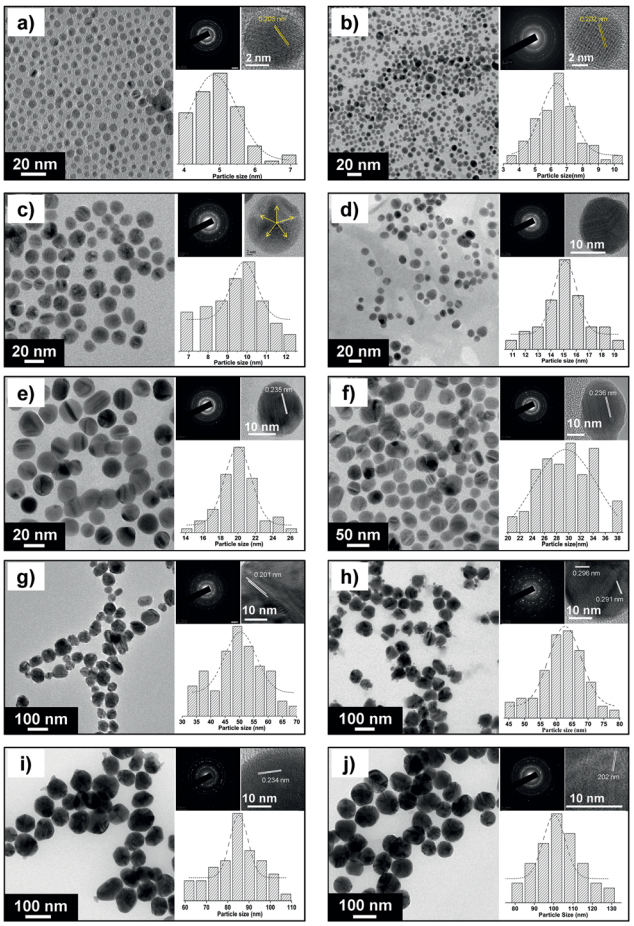

Fig. 3 FEG-TEM images of silver nanoparticles of various size ranges (a) 5 ± 0.7 nm; (b) 7 ± 1.3 nm; (c) 10 ± 2.0 nm; (d) 15 ± 2.3 nm; (e) 20 ± 2.5 nm; (f) 30 ± 5.1 nm (g) 50 ± 7.1 (h) 63 ± 7.6 (i) 85 ± 8.2 (j) 100 ± 11.2. For each image, the corresponding high resolution (HRTEM) image and lattice fringes (*d*-spacing) are shown. The histograms show the range of particle size distribution.

(see Table S5† for the exact values). For smaller nanoparticles (≤15 nm), the crystallite size matched closely with the corresponding TEM derived particle size.[35,36] This further validates our earlier discussion where the smallest nanoparticles appeared to be primarily in their monocrystalline form. However, the crystallite size was found to be less than the particle size for larger nanoparticles (*i.e.* ≥30 nm) primarily due to multiple domain diffraction caused by crystal-twinning.[36] Based on our findings, we can conclude that the AgNPs synthesized using our approach consist of a mixed population having different crystal structures as well as single-crystalline nanoparticles.

The electrostatic stabilization of various AgNPs was estimated by measuring their zeta potential values (ESI, Table S5†). The zeta potential value was found to be in the range from −26.8 to −53.1 mV for particles with an average size between 5 and 100 nm. This can be attributed to extremely high surface energies of nanoparticle suspensions. The stability of all AgNPs was tested after repeated intervals (1, 3 and 6 months) using UV-Vis and zeta potential measurements and no significant shift either in absorption peak or zeta potential values was observed. This implies that AgNPs prepared using this protocol can be stored for relatively large periods without compromising their stability.

3.2 Effect of AgNPs on bacterial growth

Dose-dependent growth kinetics of bacterial strains can be used to assess the relative rate and extent of bactericidal activity of silver nanoparticles. Fig. 4(a–c) demonstrates the growth profiles of the three representative bacterial strains treated with various concentrations of 10 nm AgNPs. The results showed that for all the bacterial strains, introduction of silver nanoparticles affected the growth kinetics as compared to the negative control (culture grown in absence of AgNPs). Bacterial growth was reduced with an increase in AgNP concentration.[14] At their respective MBC values, no visible bacterial growth was observed up to 24 hours, and thus it represents the bactericidal concentration for the specific bacterial strain. In the case of the *E. coli* MTCC 443 strain, introducing 10 and 20 μg ml^{-1} Ag(10) caused ∼18% and ∼53% reduction in bacterial density as compared to the control sample. Further, increasing concentration of AgNP to 30 and 40 μg ml^{-1} caused absence of bacterial growth as these concentrations represent the MIC and MBC values respectively, for the *E. coli* MTCC 443 strain. Interestingly, for *B. subtilis* MTCC 441, an introduction of similar concentrations of Ag(10) *i.e.*, 10 and 20 μg ml^{-1} caused a reduction of ∼38% and ∼84% in bacterial density as compared to the control sample. Another gram positive bacteria *S. aureus* NCIM 5201 caused ∼14%, ∼67%, and 97% reduction in cell density for Ag(10) concentration of 20, 40 and 80 μg ml^{-1}, respectively. Notably, the relative order of bacterial sensitivity against 10 nm sized silver nanoparticles was found to be similar as reported earlier.[32]

3.3 Size-specific antibacterial efficacy

To demonstrate the effect of the size of nanoparticles on the antibacterial effect, four bacterial strains (Gram-negative and Gram-positive, two each) were considered. The bacteriostatic and bactericidal effects of AgNPs were determined in terms of their MIC and MBC values (initial bacterial concentration, 10^5 to 10^6 CFU ml^{-1}), respectively. To the best of our knowledge, this is the first study illustrating such a detailed and systematic study regarding, relative MIC/MBC values for a wide range of size-controlled silver nanoparticles against various bacterial strains as summarized in Table 2a and b. The MIC values for different sized AgNPs were found to be in the range of 20 to 110, 60 to 160, 30 to 120, and 70 to 200 μg ml^{-1} for *E. coli* MTCC 443, *E. coli* MTCC 739, *B. subtilis* MTCC 441, and *S. aureus* NCIM 5021 bacterial strains. Similarly, the MBC values for the respective strains were found to be in the range of 30 to 140, 90 to 180, 40 to 140, and 80 to >200 μg ml^{-1}. Based on this experiment we conclude that, silver nanoparticles exhibit broad-spectrum biocidal activity towards many different microbial strains and this antibacterial effect was found to be size as well as dose dependent.

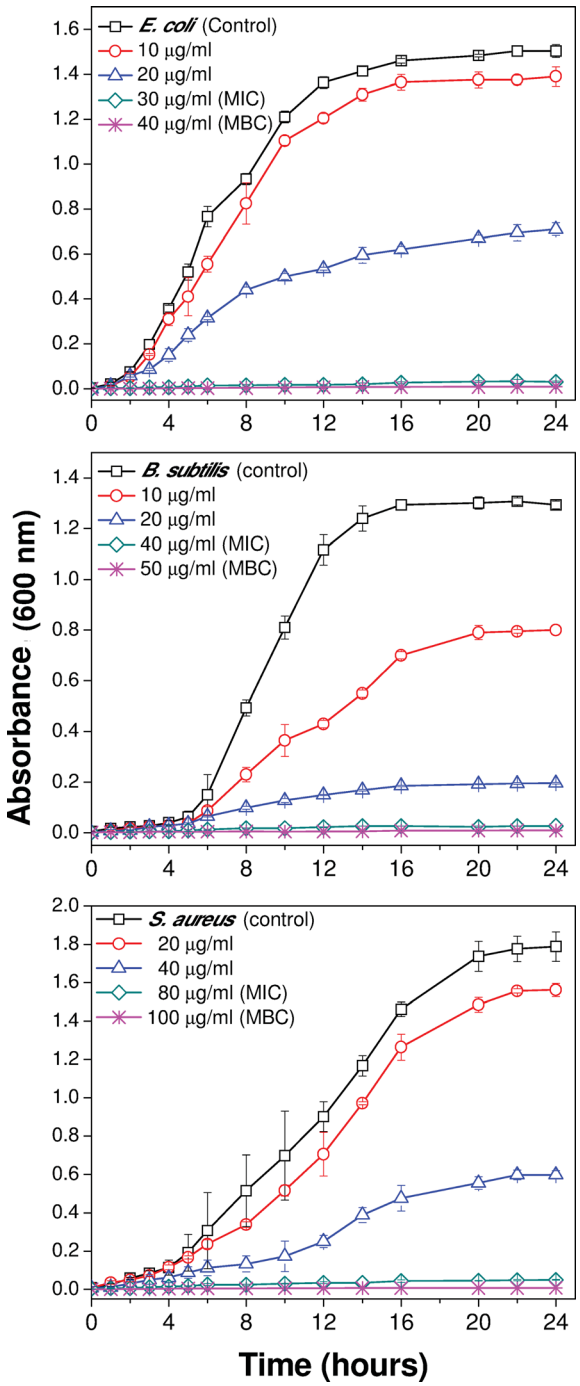

Fig. 4 Growth profile of different bacterial strains in the presence of varying concentrations of 10 nm silver nanoparticles *i.e.*, Ag(10) (a) *E. coli* MTCC 443, (b) *B. subtilis* MTCC 441 and (c) *S. aureus* NCIM 5021.

It is noteworthy that silver nanoparticles synthesized by our method demonstrated better antibacterial efficacy than other studies using nearly the same initial bacterial concentration, bacterial species and size of the nanoparticles.[32,37,38] Although Sondi and Salopek-Sondi[37] depicted effective antibacterial activity of silver nanoparticles of average size, 12.4 ± 4.2 nm against *E. coli*, even a nanoparticle concentration of 100 μg ml^{-1} could not contribute to complete growth inhibition for an initial cell concentration of 10^7 CFU ml^{-1}. In this study with initial cell concentration in the range of 10^5 to 10^6 CFU ml^{-1}, silver nanoparticles of average size 10 nm and 15 nm depicted MIC values of 30 μg ml^{-1} and 90 μg ml^{-1} for *E. coli* strain MTCC 443 and strain MTCC 739, respectively. Interestingly, for the same bacterial strains, *i.e. E. coli* MTCC 443, *E. coli* MTCC 739 and *S. aureus* NCIM 5021, Ruparelia *et al.*[32] reported relatively higher MIC values of silver nanoparticles of comparable size (40, 180 and 120 μg ml^{-1}, respectively *versus* 20, 60 and 70 μg ml^{-1} observed in this study) although the initial cell concentration was lower (10^3–10^4 CFU ml^{-1}). Even for the larger nanoparticles (100 nm), the MIC values observed in this study were much lower than those reported by Lara *et al.*[38] for silver nanoparticles of comparable size. Lara *et al.*[38] reported a MIC value of ~9000 μg ml^{-1} for the commercially manufactured AgNPs where the antibacterial tests were performed at ~10^5 CFU ml^{-1} initial bacterial concentration.

Studies by various researchers have established citrate stabilized AgNPs as an effective bactericidal nanomaterial. El-Kheshen and El-Rab[39] reported a MIC of 125 μg ml^{-1} for the citrate capped AgNPs against *E. coli* ATCC 8739 strain for an initial bacterial concentration of 10^5 to 10^6 CFU ml^{-1}. The AgNPs were found to be polydispersed in nature with a size range of 20 to 65 nm. In addition to spherical nanoparticles, rods, triangles, and irregular shapes were also reported. Thus, their antibacterial activity can not solely be explained on the basis of size, since the shape of the silver nanoparticles may have a significant effect.[14] A AgNP colloidal suspension (size, not reported) has also been used by Taner *et al.*[40] for antibacterial purposes with a reported MIC of >150 μg ml^{-1} against *E. coli* DH5α strain at ~10^8 CFU ml^{-1} initial bacterial concentration. Citrate stabilized AgNPs of varying size, *i.e.*, ~120 nm and ~160 nm exhibited variations in MIC and MBC values against multi-drug resistant bacterial strains isolated from hospital wastes for studies performed at 10^3 to 10^4 CFU ml^{-1} initial bacterial concentration.[41] For *Staphylococcus aureus* and *Bacillus megaterium*, the MIC/MBC values for these AgNPs were found to be 60/160 μg ml^{-1} and 80/160 μg ml^{-1}, respectively.

However, it was not feasible to compare all MIC/MBC values reported in different studies because of the large variation in various factors involved in the antibacterial studies, such as, variation in initial bacterial concentration, microbial strains, and composition of culture media.[32] Moreover, the size, shape, crystallinity, surface chemistry and capping agent of silver nanoparticles is likely to play a crucial role and may cause variation in the antibacterial effect.[14,16,42] Results showed that the antibacterial potential of AgNPs was greatly enhanced as their size was reduced from 100 nm to 20 nm. This effect was even more pronounced for AgNPs with a size of 10 nm and below, which favours direct contact with the bacterial cell.[13,42,43] For a particular sized AgNP, the MIC/MBC values were found to vary for different microbial strains and hence, indicate the strain-specificity in antibacterial activity.[32] Amongst the tested strains, *E. coli* MTCC 443 and *S. aureus* NCIM 5021 were found to be the most and least sensitive, respectively and this trend was also reported by other researchers.[44] *B. subtilis* MTCC 441 was found to have moderate sensitivity against the synthesized silver nanoparticles. However, the relative sensitivity cannot be

Table 2 (a) Minimum inhibitory concentration (MIC, μg ml^{-1}) and (b) minimum bactericidal concentration (MBC, μg ml^{-1}) values for silver nanoparticles of varying size[a]

(a)										
Bacterial strain	Ag(5)	Ag(7)	Ag(10)	Ag(15)	Ag(20)	Ag(30)	Ag(50)	Ag(63)	Ag(85)	Ag(100)
E. coli MTCC 443	20	20	30	30	40	50	80	90	90	110
E. coli MTCC 739	60	90	90	90	100	100	120	140	160	160
B. subtilis MTCC 441	30	40	40	50	50	60	80	90	110	120
S. aureus NCIM 5021	70	70	80	100	90	100	130	160	180	200
(b)										
E. coli MTCC 443	30	30	40	50	50	80	100	110	130	140
E. coli MTCC 739	90	100	100	110	120	120	140	170	170	180
B. subtilis MTCC 441	40	50	50	60	70	80	100	120	130	140
S. aureus NCIM 5021	80	90	100	110	100	120	160	200	>200	>200

[a] Studies were done at 10^5 to 10^6 CFU ml^{-1} initial bacterial concentrations.

explained solely on the basis of a difference in cell membrane composition, *i.e.*, Gram negative *versus* Gram positive.

Results obtained by using disk diffusion tests (Fig. 5) were also in good agreement with the MIC/MBC tests, where AgNPs up to 10 nm size showed a clear zone of inhibition (ZoI) on agar plates spread with *E. coli* MTCC 443 strain. The diameter of the ZoI was measured as 12.4 mm, 11.2 mm, 11.1 mm, and 6 mm for Ag(5), Ag(7), Ag(10), and Ag(15) impregnated disks respectively. Comparing with an earlier study, citrate capped silver nanoparticles of similar sizes (~12 nm) demonstrated a smaller width of ZoI (2.3 mm) against *E. coli*.[45] This implies that the small AgNPs synthesized using our approach have promising antibacterial potential against microorganisms. The formation of a ZoI is an indication of the bactericidal potential of sub-15 nm AgNPs, where bacteria are incapable of surviving in this zone, possibly due to release of silver (either in the form of nanoparticles or ions) from the AgNP laden disks. Beyond this zone the silver concentration was low enough to allow culture growth. In contrast, for larger nanoparticles (*i.e.*, >15 nm), a ZoI was not obtained which indicates a much inferior antibacterial activity on agar plates as compared to that in liquid medium. Besides, the release of silver from larger nanoparticles is reported to be lower,[2] the mobility of the larger sized AgNPs (>15 nm) through the semi-solid agar is also adversely affected, such that an inhibition zone was not observed.

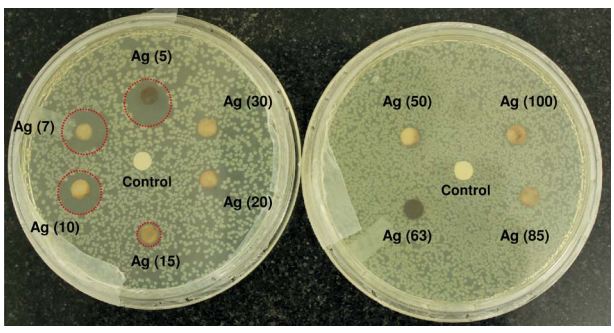

Fig. 5 Disk diffusion tests for different sized silver nanoparticles against the *E. coli* MTCC 443 strain. The zone of inhibition (ZoI) is highlighted with a dashed circle indicating a noticable antibacterial effect.

3.4 Comparative antibacterial potential at sub-10 nm scale

As mentioned earlier, the bactericidal efficacy of silver nanoparticles over a range of 5–100 nm is significantly enhanced as the size of nanoparticles is reduced below 10 nm. Therefore, a size-dependent antibacterial efficacy was tested against three bacterial strains where the nanoparticles taken were of size 5, 7 and 10 nm, designated as Ag(5), Ag(7), and Ag(10), respectively. For comparison, the concentration of individual nanoparticles was considered at their MBC concentration for a particular microbial strain, which inhibited bacterial growth. The initial bacterial concentration was adjusted to 10^5 to 10^6 CFU ml^{-1} in 50 ml nutrient broth while the time period for the antibacterial activity was evaluated up to 3 hours, as the minimum time necessary to achieve ≥99% (bacteriostatic effect) and ≥99.9% bacterial killing (bactericidal effect)[46] is expected to fall within this duration.

Fig. 6 represents the size dependent killing kinetics of Ag(5), Ag(7), and Ag(10) against the *E .coli*, *B. subtilis* and *S. aureus* bacterial strains used in earlier studies. In the case of *E. coli*, Ag(5) showed bacteriostatic (99.45% killing) and bactericidal effects (99.92% killing) in 60 and 90 minutes respectively, while Ag(7) and Ag(10) displayed almost similar bactericidal efficacy and both took almost double the time, *i.e.* 180 minutes to achieve ≥99.9% bacterial reduction. This clearly indicates that the 5 nm AgNPs mediate the fastest bactericidal action by first quickly inhibiting bacterial proliferation within 60 minutes and thereafter achieving bacterial reduction over the next half an hour. However, the extent of the bactericidal effect was found to be nearly the same for all AgNPs at sub-10 nm scale. Similarly, Ag(5) demonstrated the best antibacterial activity against *B. subtilis* by achieving bacteriostatic (99.53% killing) and bactericidal effects (99.95% killing) within 90 and 120 minutes, respectively. Silver nanoparticles of sizes 7 and 10 nm, displayed similar bactericidal efficacy and ≥99.9% bacterial reduction was observed in 180 minutes. Out of the three microbial strains tested, *S. aureus* was found to be the least sensitive against silver nanoparticles. This can be explained on the basis of the time taken to achieve the bacteriostatic effect, which was prolonged from 60 minutes for Ag(5), to 90 and 120 minutes for Ag(7), and Ag(10), respectively. It took an unexpectedly longer time (150

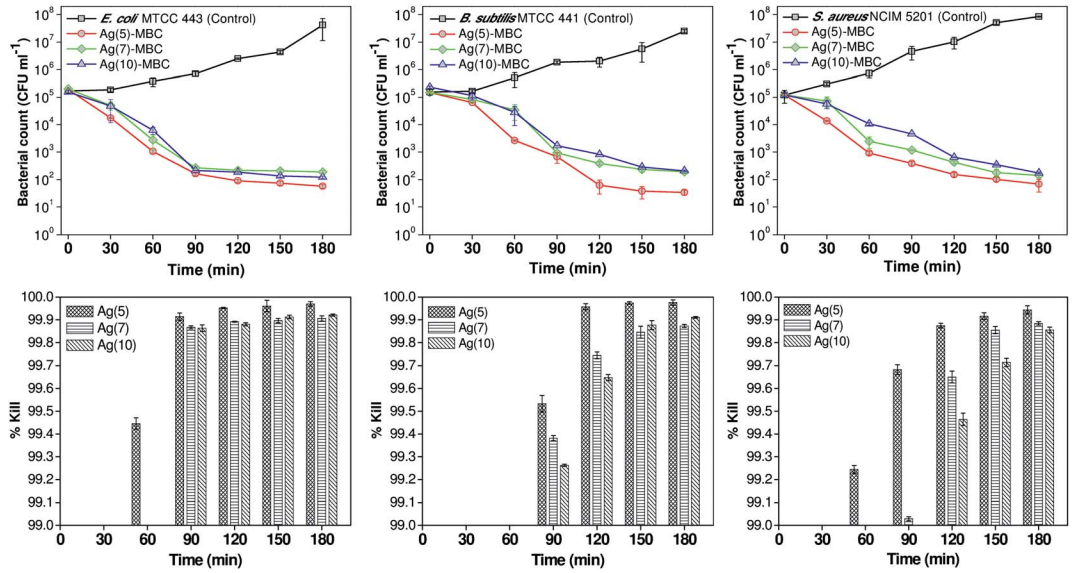

Fig. 6 Killing kinetics of various bacterial strains exposed to silver nanoparticles with average particle sizes of 5, 7 and 10 nm at their MBC values. Below each graph, the comparative efficacy of these nanoparticles when contributing to ≥99% of bacterial killing is presented.

minutes) to achieve complete reduction with Ag(5), while the bactericidal effect (*i.e.*, ≥99.9% killing) could not be achieved for Ag(7) and Ag(10) within 3 hours. However, complete killing can be expected if the duration of antibacterial studies is extended further. As defined by Kaur *et al.*,[47] the time-kill assay of Ag(5) displayed its antibacterial efficacy to be 'rapidly bactericidal' for Gram-negative, *E. coli* and 'fairly bactericidal' for the Gram-positive, *B. subtilis* and *S. aureus* strains.

The antibacterial effects of silver nanoparticles against all the bacterial strains were enhanced significantly as the particle diameter was reduced from 10 nm to 7 nm to 5 nm. This may be attributed to the enhancement in surface area to volume (SA/V) ratio with decrease in particle size. As size decreases the SA/V ratio for individual particles increases and the relative particle concentration also increases[30,42] thereby enhancing the overall SA/V ratio of AgNPs in the system. From Table 1, the calculated particle concentration (no. of particles per ml) of 5 nm AgNPs was found to be ~3.1 and ~6.7 times higher than that present in 7 nm, and 10 nm AgNPs, respectively. The theoretical total number of silver atoms present on the nanoparticles, after accounting for variable yields in these systems, were almost of the same order of magnitude (9.4×10^{18}, 8.1×10^{18}, and 11.5×10^{18}, per ml). However, in terms of antibacterial efficacy, the total number of silver atoms is less relevant than the overall SA/V ratio.

It has been reported that the nanoparticles of ~5 nm size are characterized by an excess energy at the surface as their band gap energy abruptly increases.[48] These properties are attributed to lattice contractions[49] which favor confinement of electrons and are responsible for the "electronic effects" of silver nanoparticles which thereby, enhance their direct interaction with bacterial cells.[9,48,50] Results are consistent with that of earlier studies where, the smallest AgNPs demonstrated the best antibacterial activity against both pathogenic and non-pathogenic bacterial strains, and activity was attributed to the maximum contact area associated with them.[28,51] Although, the probable reason for antibacterial activity of AgNPs cannot be fully explained by either release of Ag^+ ions or by direct contact, significant enhancement in their antibacterial effect, particularly below the 10 nm size range is predominantly attributed to the contact mode killing mechanism.[9,10,12,13,42,52]

3.5 Mechanism of bactericidal action

In support of the above discussions, the plausible role of AgNP–bacteria interactions and its antibacterial effect was further analyzed using FEG-TEM and SEM analysis (Fig. 7). Here, only *E. coli* MTCC 443 cells treated with AgNPs (~10 nm) were observed using FEG-TEM and SEM analysis. While untreated cells (Fig. 7a) appeared normal with their characteristic shape, cells treated with AgNPs (Fig. 7b) exhibited appreciable shrinkage and irregular shape. The TEM micrograph showed that AgNPs were present on the cell membrane and they appeared to be attached to the lipopolysaccharide layer present in the cell wall of Gram-negative, *E. coli* bacteria, as also reported in previous studies.[30,53] A significant number of AgNPs were also found inside the bacterial cell and this internalization of AgNPs was further confirmed in STEM (scanning tunnelling electron microscope) mode (ESI, Fig. S8†). The presence of silver inside the bacterial cell was also analyzed using EDX (Fig. 7c) and the characteristic Ag peak (~2.9 kV) was observed even after post-fixation procedures. Using FEG-SEM images, it was also found that the silver nanoparticles were invariably present all over the bacterial surface (Fig. 7d). Thus, AgNPs were present deep inside as well as on the bacterial surface.

Here, the AgNP–bacterial interaction can broadly be explained through three approaches, which may occur singly or concurrently. The first approach during their interactions can be the electrostatic attraction between negatively charged AgNPs (citrate stabilized) and positively charged residues of

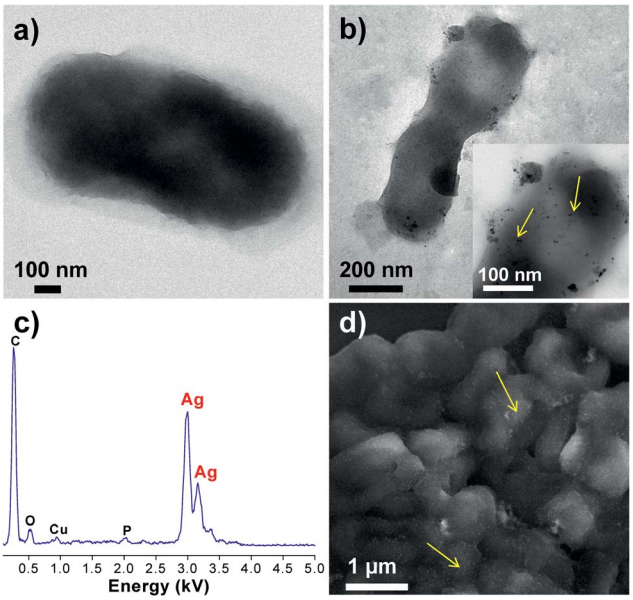

Fig. 7 FEG-TEM images of *E. coli* cells (a) untreated and (b) after treatment with silver nanoparticles. Inset shows the magnified image with the presence of silver nanoparticles, as shown by arrows. EDX analysis (c) of the bacteria shows the presence of silver. The FEG-SEM image (d) further confirms the presence of silver all over the bacterial surface.

the integral membrane proteins on the bacterial surface.[54] Another approach could be alteration in structural integrity or physicochemical changes in the bacterial cell wall. This can be explained on the basis of alteration in osmoregulation of the bacterial cell which may cause extrusion of intracellular material and may ultimately causes cell death. TEM results showed that the AgNPs caused a series of similar changes on *E. coli*. The wrinkled cell wall may indicate leakage of cytoplasmic contents outside the bacterial cell. As a third approach, AgNPs tend to penetrate through bacterial membranes,[13] and this may facilitate their internalization inside the cell. The formation of pits/holes and disruption of the bacterial cell wall can explain the evidence of AgNP internalization. After internalization, AgNPs may cause inactivation through multiple pathways, *i.e.* they may inhibit DNA replication,[54] block cellular respiration[9,25,32] and may cause ROS generations.[49] These mechanisms may occur in parallel and contribute towards quick antibacterial effect.

However, it will require further efforts to elucidate whether the antibacterial effect of AgNPs, particularly those below 10 nm, is entirely driven by direct cell–AgNP contact or by the release of Ag^+ ions which could also play an important role. Perhaps an initial AgNP–bacterial contact may trigger the principal antibacterial mechanism by facilitating the entry of AgNPs inside the bacterial cells followed by a burst release of silver ions inside the bacterial cells just sufficient to cause the bactericidal effect. Therefore, the hypothesis of a synergistic mechanism between contact killing and silver release should not be overlooked. Further studies are needed to explore the above possibilities.

4. Conclusions

Synthesis of AgNPs by a common synthetic protocol which is facile and offers AgNPs with tunable sizes and low dispersivity is a significant contribution. All AgNPs were found to be highly toxic to the bacterial strains and their antibacterial efficacy increased with lowering particle size. This effect was significantly enhanced as the size of nanoparticles approached the sub-10 nm range and, 5 nm AgNPs demonstrated the fastest bactericidal activity as compared to 7 nm and 10 nm AgNPs at their respective, MBC dosage. Interestingly, the extent of bactericidal activity was found to be the same for 5, 7 and 10 nm AgNPs irrespective of the bacterial strains used in this study. The variation in their antibacterial effect therefore, could be related to the particle concentration of the AgNP suspension. Microscopic analysis of *E. coli* cells treated with the AgNPs illustrated their interaction with the cell wall, which facilitated their subsequent entry inside the cells. Silver nanoparticles of 8.6 nm average size synthesized using the current protocol have been successfully immobilized on a surface functionalized silica support for water disinfection application.[12] While this study has illustrated the antibacterial efficacy of free silver nanoparticles, subsequent studies may illustrate the effect of size controlled AgNPs immobilized on a support. We believe that along with the water disinfection application, these AgNPs may be utilized effectively as a nano-coating for surgical devices, instruments and wound healing bandages.

Acknowledgements

The authors gratefully acknowledge Sophisticated Analytical Instrument Facility (SAIF), and IIT-Bombay central facility (XRD, Zeta potential, ICP-AES, and FEG-TEM) for the characterization studies. This study was partially funded by Nanomission, DST, Govt. of India.

References

1 C. N. R. Rao, G. U. Kulkarni, P. J. Thomas and P. P. Edwards, *Chem.–Eur. J.*, 2002, **8**, 28–35.
2 Z. Xiu, Q. Zhang, H. L. Puppala, V. L. Colvin and P. J. J. Alvarez, *Nano Lett.*, 2012, **12**, 4271–4275.
3 Woodrow Wilson Database, *An inventory of nanotechnology-based consumer products currently on the market*, 2011, http://www.nanotechproject.org/inventories/consumer/analysis_draft/.
4 S. Asghari, S. A. Johari, J. H. Lee, Y. S. Kim, Y. B. Jeon, H. J. Choi, M. C. Moon and I. J. Yu, *J. Nanobiotechnol.*, 2012, **10**, 14.
5 Y. Sun and Y. Xia, *Science*, 2002, **298**, 2176–2179.
6 L. Bois, F. Chassagneux, C. Desroches, Y. Battie, N. Destouches, N. Gilon, S. Parola and O. Stéphan, *Langmuir*, 2010, **26**, 8729–8736.
7 X. Dong, X. Ji, H. Wu, L. Zhao, J. Li and W. Yang, *J. Phys. Chem. C*, 2009, **113**, 6573–6576.
8 J. Thiel, L. Pakstis, S. Buzby, M. Raffi, C. Ni, D. J. Pochan and S. I. Shah, *Small*, 2007, **3**, 799–803.

9 C. N. Lok, C. M. Ho, R. Chen, Q. Y. He, W. Y. Yu, H. Sun, P. K. H. Tam, J. F. Chiu and C. M. Che, *J. Proteome Res.*, 2006, **5**, 916–924.
10 P. Gunawan, C. Guan, X. Song, Q. Zhang, S. S. J. Leong, C. Tang, Y. Chen, M. B. Chan-park, M. W. Chang, K. Wang and R. Xu, *ACS Nano*, 2011, **5**, 10033–10040.
11 D. R. Monteiro, L. F. Gorup, A. S. Takamia, A. C. Ruvollo-Filho, E. R. De Camargo and D. B. Barbosa, *Int. J. Antimicrob. Agents*, 2009, **34**, 103–110.
12 S. Agnihotri, S. Mukherji and S. Mukherji, *Nanoscale*, 2013, **5**, 7328–7340.
13 J. R. Morones, J. L. Elechiguerra, A. Camacho, K. Holt, J. B. Kouri, J. T. Ramírez and M. J. Yacaman, *Nanotechnology*, 2005, **16**, 2346–2353.
14 S. Pal, Y. K. Tak and J. M. Song, *Appl. Environ. Microbiol.*, 2007, **73**, 1712–1720.
15 S. Agnihotri, S. Mukherji and S. Mukherji, *Appl. Nanosci.*, 2012, **2**, 179–188.
16 S. Mukherji, J. P. Ruparelia and S. Agnihotri, in *Nano-Antimicrobials: Progress and Prospects*, ed. N. Cioffi and M. Rai, Springer Verlag, Berlin Heidelberg, 2012, pp. 225–251.
17 D. Steinigeweg and S. Schlücker, *Chem. Commun.*, 2012, **48**, 8682–8684.
18 X. Z. Lin, X. Teng and H. Yang, *Langmuir*, 2003, **19**, 10081–10085.
19 N. Shirtcliffe, U. Nickel and S. Schneider, *J. Colloid Interface Sci.*, 1999, **211**, 122–129.
20 K. K. Caswell, C. M. Bender and C. J. Murphy, *Nano Lett.*, 2003, **3**, 667–669.
21 Y. Tan, X. Dai, Y. Li and D. Zhu, *J. Mater. Chem.*, 2003, **13**, 1069–1075.
22 J. Yang, H. Yin, J. Jia and Y. Wei, *Langmuir*, 2011, **27**, 5047–5053.
23 J. A. Creighton, C. G. Blatchford and M. G. Albrecht, *J. Chem. Soc., Faraday Trans. 2*, 1979, **75**, 790–798.
24 A. Pyatenko, M. Yamaguchi and M. Suzuki, *J. Phys. Chem. C*, 2007, **111**, 7910–7917.
25 V. K. Sharma, R. A. Yngard and Y. Lin, *Adv. Colloid Interface Sci.*, 2009, **145**, 83–96.
26 R. R. Arvizo, S. Bhattacharyya, R. A. Kudgus, K. Giri, R. Bhattacharya and P. Mukherjee, *Chem. Soc. Rev.*, 2012, **41**, 2943–2970.
27 Y. Ma and Y. Qu, *Nanoscale*, 2012, **4**, 3036–3039.
28 G. A. Martinez-Castanon, N. Nino-Martinez, F. Martinez-Gutierrez, J. R. Martinez-Mendoza and F. Ruiz, *J. Nanopart. Res.*, 2008, **10**, 1343–1348.
29 H. L. Liu, S. A. Dai, K. Y. Fu and S. H. Hsu, *Int. J. Nanomed.*, 2010, **5**, 1017–1028.
30 M. E. Samberg, P. E. Orndorff and N. A. Monteiro-Riviere, *Nanotoxicology*, 2011, **5**, 244–253.
31 V. D. Lago, L. F. de Oliveira, K. de A. Gonçalves, J. Kobarg and M. B. Cardoso, *J. Mater. Chem.*, 2011, **21**, 12267–12273.
32 J. P. Ruparelia, A. K. Chatterjee, S. P. Duttagupta and S. Mukherji, *Acta Biomater.*, 2008, **4**, 707–716.
33 X. C. Jiang, S. X. Xiong, Z. A. Tian, C. Y. Chen, W. M. Chen and A. B. Yu, *J. Phys. Chem. C*, 2011, **115**, 1800–1810.
34 M. Chen, Y. G. Feng, X. Wang, T. C. Li, J. Y. Zhang and D. J. Qian, *Langmuir*, 2007, **23**, 5296–5304.
35 H. Borchert, E. V. Shevchenko, A. Robert, I. Mekis, A. Kornowski, G. Grübel and H. Weller, *Langmuir*, 2005, **21**, 1931–1936.
36 R. Ma, C. Levard, S. M. Marinakos, Y. Cheng, J. Liu, F. M. Michel, G. E. Brown and G. V. Lowry, *Environ. Sci. Technol.*, 2012, **46**, 752–759.
37 I. Sondi and B. Salopek-Sondi, *J. Colloid Interface Sci.*, 2004, **275**, 177–182.
38 H. H. Lara, N. V. Ayala-Núnez, L. D. C. I. Turrent and C. R. Padilla, *World J. Microbiol. Biotechnol.*, 2010, **26**, 615–621.
39 A. A. El-Kheshen and S. F. G. El-Rab, *Pharma Chem.*, 2012, **4**, 53–65.
40 M. Taner, N. Sayar, I. G. Yulug and S. Suzer, *J. Mater. Chem.*, 2011, **21**, 13150–13154.
41 D. Borah, P. Deka, P. Bhattacharjee, A. Changmai and R. N. S. Yadav, *J. Pharm. Res.*, 2013, **7**, 478–482.
42 C. N. Lok, C. M. Ho, R. Chen, Q. Y. He, W. Y. Yu, H. Sun, P. K. H. Tam, J. F. Chiu and C. M. Che, *JBIC, J. Biol. Inorg. Chem.*, 2007, **12**, 527–534.
43 M. B. Ahmad, J. J. Lim, K. Shameli, N. A. Ibrahim, M. Y. Tay and B. W. Chieng, *Chem. Cent. J.*, 2012, **6**, 101–109.
44 J. S. Kim, E. Kuk, K. N. Yu, J. H. Kim, S. J. Park, H. J. Lee, S. H. Kim, Y. K. Park, Y. H. Park, C. Y. Hwang, Y. K. Kim, Y. S. Lee, D. H. Jeong and M. H. Cho, *Nanomed.: Nanotechnol., Biol. Med.*, 2007, **3**, 95–101.
45 A. S. Nair, N. P. Binoy, S. Ramakrishna, T. R. R. Kurup, L. W. Chan, C. H. Goh, Md. R. Islam, T. Utschig and T. Pradeep, *ACS Appl. Mater. Interfaces*, 2009, **1**, 2413–2419.
46 G. A. Pankey and L. D. Sabath, *Clin. Infect. Dis.*, 2004, **38**, 864–870.
47 P. Kaur, S. Agarwal and S. Datta, *PLoS One*, 2009, **4**, e5923.
48 M. Auffan, J. Rose, J. Y. Bottero, G. V. Lowry, J. P. Jolivet and M. R. Wiesner, *Nat. Nanotechnol.*, 2009, **4**, 634–641.
49 A. Nel, T. Xia, L. Mädler and N. Li, *Science*, 2006, **311**, 622–627.
50 F. Raimondi, G. G. Scherer, R. Kötz and A. Wokaun, *Angew. Chem., Int. Ed.*, 2005, **44**, 2190–2209.
51 Z. Lu, K. Rong, J. Li, H. Yang and R. Chen, *J. Mater. Sci.: Mater. Med.*, 2013, **24**, 1465–1471.
52 A. Dror-Ehre, H. Mamane, T. Belenkova, G. Markovich and A. Adin, *J. Colloid Interface Sci.*, 2009, **339**, 521–526.
53 X. H. N. Xu, W. J. Brownlow, S. V. Kyriacou, Q. Wan and J. J. Viola, *Biochemistry*, 2004, **43**, 10400–10413.
54 D. M. Eby, H. R. Luckarift and G. R. Johnson, *ACS Appl. Mater. Interfaces*, 2009, **1**, 1553–1560.